



NJC

Tuning the optical and electrochemical properties of core-substituted naphthalenediimides with styryl imide substituent

Journal:	<i>New Journal of Chemistry</i>
Manuscript ID:	NJ-ART-09-2014-001645.R2
Article Type:	Paper
Date Submitted by the Author:	30-Dec-2014
Complete List of Authors:	Fernando, Roshan; Case Western Reserve University, Chemistry Etheridge, Forrest; Case Western Reserve University, Chemistry Muller, Evan; Case Western Reserve University, Chemistry Sauve, Genevieve; Case Western Reserve University, Chemistry

SCHOLARONE™
Manuscripts

Tuning the optical and electrochemical properties of core-substituted naphthalenediimides with styryl imide substituent

Roshan Fernando, Forrest Etheridge, Evan Muller, Geneviève Sauvé*

Department of Chemistry, Case Western Reserve University, Cleveland, Ohio 44106, United States

Abstract

The effect of styryl imide substitution on optical and electrochemical properties of core-substituted naphthalenediimides was examined by synthesizing a series of naphthalenediimide molecules. 2-Ethylhexylamino and 5-(2-ethylhexyl)thiophene groups were used as core substituents. The optical and electrochemical properties of styryl imide substituted compounds were compared with other imide substitutions including hydrogen, 2-ethylhexyl, and 4-thienylphenyl. Generally, the imide substituents had little effect on the optical properties, except when the combination of alkylamino core and styryl imide substituents was used. In this latter case, we observed a 104 nm red-shift of the absorption onset upon film formation, resulting in an unusually broad visible absorption (500-800 nm) for these types of molecules. This is explained by the planarity of the molecule and the formation of intermolecular aromatic donor-acceptor type interactions. These results show that imide substituents play a role in tuning opto-electronic properties of NDI molecules, and that NDI molecules with styryl imide substituents merit further evaluation for opto-electronic applications.

Introduction

Arylene diimides are planar conjugated molecules with high electron affinity that can be easily reduced to the anion or dianion.^{1,2} Many are colorful and have been used as stable dyes, as well as n-type organic semiconductors in organic electronic applications (e.g. organic field-effect transistors, photovoltaics, light emitting diode) and as electron acceptors in artificial photosystems. To further their use in various opto-electronic applications, it is important to understand how to tune their frontier orbital energy levels, as

well as their optical and electrochemical properties. These properties of arylene diimides are very sensitive to the aromatic core size and core substitution,¹ but are not typically sensitive to imide-substituents. An interesting exception is with the smallest core diimide, naphthalenediimide (NDI), whose 1st reduction potential could be tuned via the imide substituent: Relative to the imide alkyl group, alkylphenyl and phenylthienyl substituents shifted the reduction potential anodically by as much as 120 mV.^{3,4} To rationalize these observations, the authors suggested that the aromatic rings adjacent to the imide nitrogen have electron accepting properties and can lower the charge density at the reduction sites through delocalization, thus facilitating reduction and stabilizing the radical anion.³ The reduction sites in arylene diimides are thought to be mainly localized on the imide groups, most likely residing on the carbonyl oxygen due to the electron-withdrawing nature of oxygen.⁵ These results triggered two questions: 1) Could we use a combination of core and imide substituents to fine tune the opto-electronic properties of NDI, and 2) Would using an imide group that is in plane with the NDI core have a greater impact on the opto-electronic properties of NDI than phenyl groups, which are perpendicular to the NDI core?

To investigate these questions, we designed a series of NDI compounds shown in Chart 1. We chose to study core 2,6-dialkylamino NDI and 2,6-dithiophene NDI because of their particular interest to opto-electronic and solar energy conversion applications due to their strong absorption band at 610 nm and 525 nm, respectively.^{6,7} To investigate the effect of the imide substituent on the opto-electronic properties, we synthesized two series with various imide substituents: the RF7 series (RF are the first author's initials) have thiophene core groups while the RF8 series have alkylamino core groups. The imide substituents studied are hydrogen (H), 2-ethylhexyl (a) and styryl (b). The styryl group was chosen because of its ability to lie in plane with the NDI core and its ability to accept electron density from the imide group through delocalization. For the 2,6-alkylamino NDI, we also compare the styryl imide substituent with the 4-thienylphenyl substituent, RF6,⁸ since 4-thienylphenyl lies perpendicular to the NDI core. The optical and electrochemical properties were studied and explained using DFT calculations.

Interestingly, the imide substituents had a much smaller effect on the reduction potentials of core-substituted NDI than on non core substituted NDI molecules, suggesting that the effect of the core substituents can override those of the imide substituent. The dihedral angle between the NDI core and the imide substituent had a large impact on the solid-state optical properties. The film of RF8b had a broader absorption and lower optical gap than RF6, due to a combination of increased planarity and donor-acceptor character of the NDI and imide substituent.

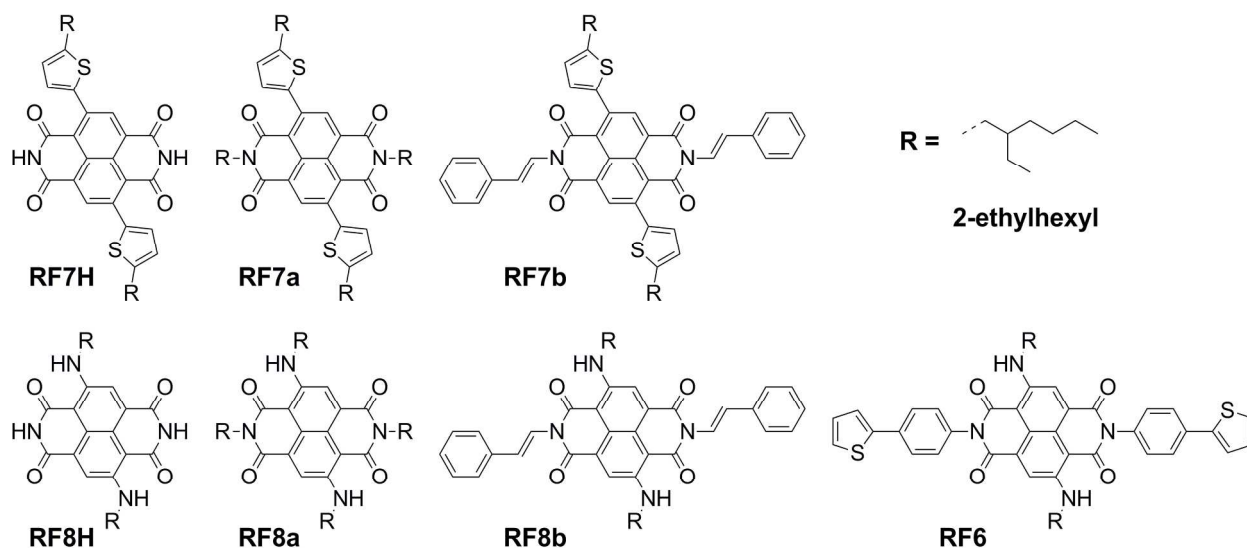


Chart 1 Six core-substituted NDI molecules with different imide substituents studied. (R = 2-ethylhexyl for all compounds)

Experimental Section

Materials

1,4,5,8-Naphthalenetetracarboxylic dianhydride (Aldrich), 2-ethylhexylamine (Aldrich), thiophene (Aldrich), trimethylstannyl chloride (Aldrich), butyl lithium (Aldrich), *trans*-2-phenylvinylboronic acid (Aldrich), dibromoisocyanuric acid (TCI America) were used as received. All other reagents and solvents were used as received unless otherwise specified. 2-(2-Ethylhexyl)-5-trimethylstannylthiophene was synthesized starting with thiophene following literature procedures.^{9,10} 2,6-Dibromo-1,4,5,8-

tetracarboxylicnaphthalenedianhydride (26BrNDA) was synthesized from 1,4,5,8-tetracarboxylicnaphthalenedianhydride (NDA) and 2,6-dibromo-1,4,5,8-tetracarboxylicnaphthalenediimide (26BrNDI) were synthesized following literature procedures and the latter was used without any purification.^{11,12} N,N-Di(2-ethylhexylamino)-2,6-di(2-ethylhexylamino)-1,4,5,8-tetracarboxydiimide (RF8a) was synthesized following a literature procedure.¹³

Methods

¹H-NMR spectra were recorded using a Varian 400 MHz spectrometer. Chemical shifts are reported in parts per million relative to CDCl₃ (7.26 ppm), CD₂Cl₂ (5.32 ppm), d⁶-DMSO (2.50 ppm) or d⁵-pyridine (8.74 ppm). MALDI-TOF MS spectra were acquired in reflective negative ion mode; samples were prepared from chloroform solutions using terthiophene as the matrix. UV-vis absorption spectra were collected on a Cary50 spectrophotometer. UV-vis spectra were obtained for chloroform (HPLC grade) solutions or for spin-coated films on glass substrates. The films were spin-coated from chloroform solutions (30 mg/mL) at 600 rpm for 60 s. The absorption spectra of films were corrected for scattering and details of corrections are available in supporting information. Emission spectra were collected in chloroform solutions using a Cary500 spectrofluorometer. Cyclic voltammetry measurements were performed at room temperature using 0.1 M Bu₄NPF₆ in dry dichloromethane (distilled over CaH₂) as the electrolyte and ferrocene as the internal standard. The solutions were purged with dry nitrogen for 10 min prior to the measurement. Glassy carbon (GC) working electrodes were polished with 0.05 μm alumina, thoroughly cleaned and dried. Platinum wires were used as the counter and reference electrodes. All scans were performed at a scan rate of 0.1 V/s. The E_{1/2} values vs ferrocene/ferrocenium (Fc/Fc⁺) were calculated by setting the E_{1/2} of Fc/Fc⁺ to 0.0 V.

Density functional theory (DFT) calculations were done both in gas phase and in chloroform solution using Gaussian 09 software package¹⁴ and visualized using Gaussview software.¹⁵ The B3LYP^{16,17} hybrid DFT level and 6-31G(d,p) basis set (for all atoms) were used for the entire study.

Polarizable continuum model (PCM) was used as the solvent model. Optimized geometries were recognized as local minima by frequency calculations.

Synthesis

2,6-Dibromonaphthalene-1,4,5,8-tetracarboxylic dianhydride (26BrNDA). 1,4,5,8-

Naphthalenetetracarboxylic dianhydride (1 g) was brominated at the 2nd and 6th positions following the literature procedure.¹¹ The crude product was washed with acetone and methanol to give the product as a bright yellow solid. Yield: 0.54 g, 33 %. ¹H-NMR (400 MHz, d⁶-DMSO), δ , ppm): 8.79 (s, 1H).

Elemental analysis: Anal. Calcd for C₁₄H₂Br₂O₆: C, 39.47; H, 0.47. Found: C, 39.22; H, 0.71.

2,6-Dibromonaphthalene-1,4,5,8-tetracarboxydiimide (26BrNDI). This was synthesized following a literature procedure.¹² Starting with 26BrNDA (1 g), the product was isolated as an orange-yellow solid (0.83 g). Although proton NMR showed some impurities, the product was used without further purification in the proceeding steps. ¹H-NMR (400 MHz, d⁶-DMSO), δ , ppm): 12.28 (s, 1H), 8.64 (s, 1H).

2,6-Di(5-(2-ethylhexylthiophen-2-yl))-1,4,5,8-tetracarboxydiimide (RF7H). 2,6-Dibromo-1,4,5,8-tetracarboxydiimide (1.70 g, 4 mmol), 2-(2-ethylhexyl)-5-trimethylstannylthiophene (2.90 g, 8 mmol), tetrakis(triphenylphosphino)palladium(0) (0.46 g, 10% mmol) were stirred in anhydrous chlorobenzene at 70 °C for 24 h under nitrogen. After cooling to room temperature, the mixture was dissolved in dichloromethane (250 mL) and filtered through a Celite plug. The filtrate was then concentrated under reduced pressure and a precipitate was formed by pouring into methanol (500 mL). The precipitate was collected by vacuum filtration and washed thoroughly with acetone and methanol. The dried crude product was then purified by silicagel column using 10% ethyl acetate in dichloromethane as the eluent. The final product was obtained as a dark purple solid. Yield: 0.52 g, 20%. ¹H-NMR (400 MHz, d⁶-DMSO), δ , ppm): 11.99 (s, 2H), 8.40 (s, 2H), 7.31 – 7.30 (d, J = 4.0 Hz, 2H), 6.92 – 6.91 (d, J = 4.0 Hz, 2H), 2.83 – 2.82 (d, J = 4.0 Hz, 4H), 1.68 – 1.55 (m, 2H), 1.42 – 1.20 (m, 16H), 0.92 – 0.86 (m, 12H).

MALDI-TOF-MS: m/z 653.33 [M-H]⁻. Elemental analysis: Anal. Calcd for C₃₈H₄₂N₂O₄S₂: C, 69.69; H, 6.46; N, 4.28. Found: C, 69.84; H, 6.49; N, 4.07.

2,6-Di(2-ethylhexylamino)-1,4,5,8-tetracarboxydiimide (RF8H). 2,6-Dibromo-1,4,5,8-tetracarboxydiimide (0.901 g, 2.1 mmol) was refluxed in 2-ethylhexylamine (20 mL, 122.1 mmol) solution for 2 h at 145 °C in a dry round bottom flask equipped with a condenser under nitrogen atmosphere. After cooling to room temperature, the mixture was poured into methanol and approximately 10 mL of glacial acetic acid was added. The mixture was filtered and the solid precipitate was collected and purified by Soxhlet extraction following the solvent sequence methanol (40 h), acetonitrile (10 h) and tetrahydrofuran (THF) (10 h). The product was isolated from the THF fraction by precipitation in methanol as a blue solid. Yield: 0.67 g, 60%. ¹H-NMR (400 MHz, *d*⁵-pyridine), δ, ppm): 13.82 (s, 2H), 9.80 – 9.78 (t, J = 4.0 Hz, 2H), 8.45 (s, 2H), 3.41 – 3.39 (t, J = 4.0 Hz, 4H), 1.76 – 1.70 (m, 2H), 1.57 – 1.40 (m, 8H), 1.33 – 1.23 (m, 8H), 0.96 – 0.92 (t, J = 8.0 Hz, 6H), 0.91 – 0.88 (t, J = 6.0 Hz, 6H). MALDI-TOF-MS: m/z 519.27 [M-H]⁻. Elemental analysis: Anal. Calcd for C₃₀H₄₀N₄O₄: C, 69.20; H, 7.74; N, 10.76. Found: C, 68.98; H, 7.54; N, 10.72.

N,N'-Di(2-ethylhexyl)-2,6-di(5-(2-ethylhexylthiophen-2-yl))-1,4,5,8-tetracarboxydiimide (RF7a). 2,6-Dibromo-1,4,5,8-tetracarboxylic dianhydride (26BrNDA) (0.90 g, 2.11 mmol) and 2-ethylhexylamine (2.08 mL, 6 mol equivalent) were refluxed in glacial acetic acid for 1 h. After cooling to room temperature, an orange solid was collected by vacuum filtration and washed with acetic acid, acetone and diethyl ether. After drying under vacuum overnight, an orange solid (0.96 g) was obtained. Then, 0.40 g (0.88 mmol compared to 26BrNDA) of this crude product and 2-(2-ethylhexyl)-5-trimethylstannylthiophene (0.467 g, 1.30 mmol) with 5 % mol tetrakis(triphenylphosphino)palladium(0) were reacted under Suzuki coupling conditions similarly to the synthesis of RF7H. The crude product was purified by column chromatography using silicagel with 30% hexanes in dichloromethane as the eluent. The final product was obtained as an orange-red solid. Yield: 0.32 g, 42%. ¹H-NMR (400 MHz, CDCl₃), δ, ppm): 8.75 (s, 2H), 7.18 – 7.17 (d, J = 4.0 Hz, 2H), 6.84 – 6.83 (d, J = 4.0 Hz, 2H), 4.10 – 4.07 (m, 4H), 2.85 – 2.83 (d, J = 8.0 Hz, 4H), 1.95 – 1.87 (m, 2H), 1.68 – 1.60 (m, 2H), 1.45 – 1.23 (m, 32H), 0.95

– 0.85 (m, 24H). MALDI-TOF-MS: m/z 877.33 [M-H]⁺. Elemental analysis: Anal. Calcd for C₅₄H₇₄N₂O₄S₂: C, 73.76; H, 8.48; N, 3.19. Found: C, 73.76; H, 7.87; N, 3.20.

N,N'-Di(2-ethylhexyl)-2,6-di(2-ethylhexylamino)-1,4,5,8-tetracarboxydiimide (RF8a). This was synthesized according to the literature procedure.¹³ Final product is a blue solid. Yield: 25%. ¹H-NMR (400 MHz, CDCl₃), δ , ppm): 9.45 – 9.42 (t, J = 6.0 Hz, 2H), 8.17 (s, 2H), 4.18 – 4.08 (m, 4H), 3.43 – 3.40 (t, J = 6.0 Hz, 4H), 1.97 – 1.92 (m, 2H), 1.78 – 1.74 (m, 2H), 1.56 – 1.27 (m, 32H), 0.99 – 0.86 (m, 24H). MALDI-TOF-MS: m/z 743.78 [M-H]⁺. Elemental analysis: Anal. Calcd for C₄₆H₇₂N₄O₄: C, 74.15; H, 9.74; N, 7.52. Found: C, 74.43; H, 9.70; N, 7.40.

N,N'-Distyryl-2,6-di(5-(2-ethylhexylthiophen-2-yl))-1,4,5,8-tetracarboxydiimide (RF7b). 2,6-Di(5-(2-ethylhexylthiophen-2-yl))-1,4,5,8-tetracarboxydiimide (RF7H) (0.50 g / 0.76 mmol), trans-2-phenylvinylboronic acid (0.45 g / 3.05 mmol), copper (II) acetate (0.28 g / 1.53 mmol), triethylamine (0.4 mL) and 4 Å ms were stirred in dichloromethane (40 mL) in a round bottom flask at room temperature for 1 h. The reaction was monitored by thin layer chromatography with dichloromethane as the eluent. A solid crude product was collected by pouring the reaction mixture into methanol (250 mL) followed by vacuum filtration. After drying under vacuum overnight, pure product was isolated by column chromatography using silicagel and dichloromethane as eluent. The dried final product was a dark orange-red solid. Yield: 0.15 g, 23%. ¹H-NMR (400 MHz, CD₂Cl₂), δ , ppm): 8.80 (s, 2H), 7.51 – 7.29 (m, 14H), 7.25 – 7.24 (d, J = 4.0 Hz, 2H), 6.89 – 6.88 (d, J = 4.0 Hz, 2H), 2.89 – 2.87 (d, J = 8.0 Hz, 4H), 1.70 – 1.63 (m, 2H), 1.49 – 1.20 (m, 16H), 0.96 – 0.88 (m, 12H). MALDI-TOF-MS: m/z 857.18 [M-H]⁺. Elemental analysis: Anal. Calcd for C₅₄H₅₄N₂O₄S₂: C, 75.49; H, 6.34; N, 3.26. Found: C, 75.78; H, 6.30; N, 3.15.

N,N'-Distyryl-2,6-di(2-ethylhexylamino)-1,4,5,8-tetracarboxydiimide (RF8b). 2,6-Di(2-ethylhexylamino)-1,4,5,8-tetracarboxydiimide (RF8H) (50 mg / 0.096 mmol), trans-2-phenylvinylboronic acid (36 mg / 0.243 mmol), copper (II) acetate (52 mg / 0.286 mmol), triethylamine (0.05 mL) and 4 Å ms were

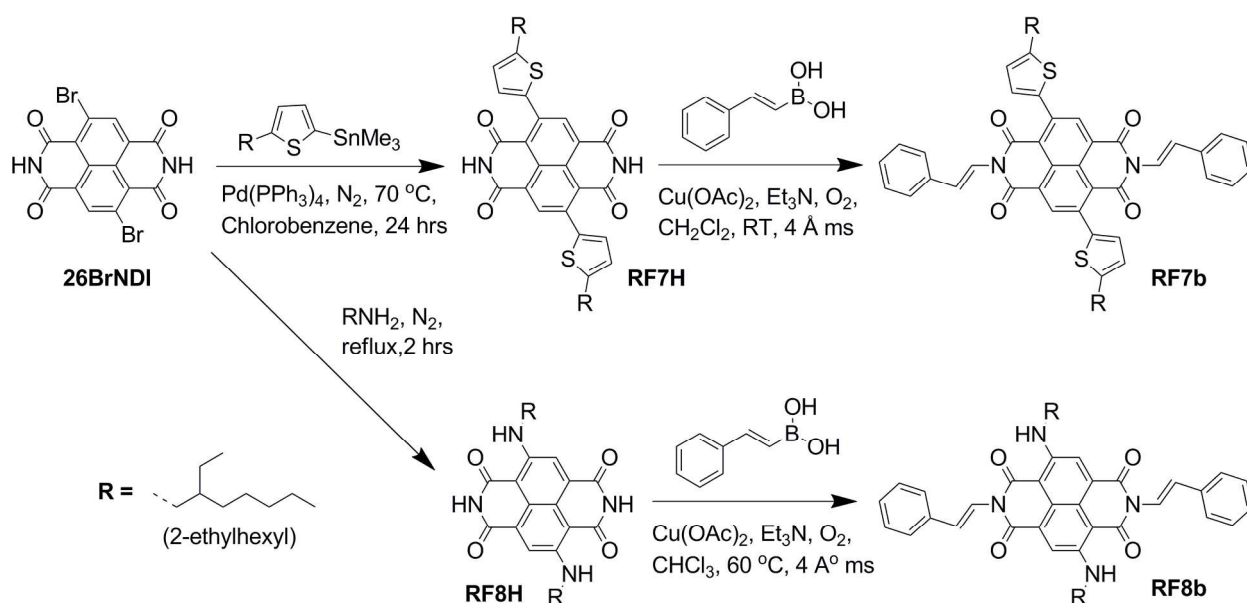
refluxed in chloroform (10 mL, HPLC grade) in a round bottom flask under oxygen. The reaction was monitored by thin layer chromatography with dichloromethane as the eluent. After 24 h, trans-2-phenylvinylboronic acid (18 mg), copper (II) acetate (26 mg) and triethylamine (0.05 mL) were added and refluxed for another 24 h under the same conditions. After cooling to room temperature, the mixture was poured into methanol (100 mL) and a dark blue solid was collected by vacuum filtration and vacuum dried overnight. The final product was isolated by column chromatography using silicagel with dichloromethane as the eluent. The dried final product was a dark purple-blue solid. Yield: 6 mg, 8.6%. $^1\text{H-NMR}$ (400 MHz, CD_2Cl_2), δ , ppm): 9.39 – 9.36 (t, $J = 6.0$ Hz, 2H), 8.11 (s, 2H), 7.56 – 7.30 (m, 14H), 3.44 – 3.41 (m, 4H), 1.79 – 1.71 (m, 2H), 1.58 – 1.20 (m, 16H), 0.99 – 0.80 (m, 12H). MALDI-TOF-MS: m/z 723.34 [M-H] $^-$. Elemental analysis: Anal. Calcd for $\text{C}_{46}\text{H}_{52}\text{N}_4\text{O}_4$: C, 76.21; H, 7.23; N, 7.73. Found: C, 76.79; H, 7.51; N, 6.87.

Results and Discussion

Synthesis

Scheme 1 shows the synthesis of the core-substituted NDI compounds. Core-substituted NDI compounds with alkyl imide groups were synthesized based on literature procedures.⁷ The thiophene core-substituted compound, RF7a, was isolated as an orange-red solid, whereas the alkylamino core substituted compound, RF8a, was isolated as a blue solid. To synthesize the thiophene core-substituted NDI with styryl imide substituent, RF7b, the bromine core substituents of 26BrNDI were first substituted with 5-(2-ethylhexyl)thiophene by Stille coupling reaction in 20% yield to give RF7H. RF7H was then subjected to Chan-Lam coupling¹⁸⁻²¹ conditions with trans-2-phenylvinylboronic acid following a published procedure for phthalimides.²² The final product was purified by column chromatography to give an orange-red solid. The synthesis of alkylamino core-substituted NDI with the styryl imide substituent, RF8b, proved to be more challenging. The bromines of 26BrNDI were easily substituted with 2-ethylhexylamine by aromatic nucleophilic substitution to give RF8H in 60% yield. However, RF8H

could not be purified by column chromatography due to its limited solubility in organic solvents. Instead, it was purified by Soxhlet extractions using methanol, acetonitrile and tetrahydrofuran (THF), with the product being recovered from the THF fraction. The Chan-Lam coupling conditions used to make RF7b did not work for synthesizing RF8b due to the limited solubility of RF8H in dichloromethane. We found that THF or chloroform worked better (Table S1), giving the desired RF8b product as a dark purple-blue solid. All final compounds were characterized by NMR, mass spectroscopy and elemental analysis, and found to be pure.



Scheme 1 Synthesis of RF7H, RF8H, RF7b and RF8b.

Optical properties .

The optical properties of RF7a and RF8a in solution, summarized in Table 1, are in agreement with the literature for similar core-substituted NDI with alkyl imide substituents:^{7,8,23} the low energy absorption maxima were 524 nm and 625 nm, and the emission maxima were 625 nm and 653 nm for RF7a and RF8a, respectively. Figure 1A compares the absorption spectra of the RF7 series (thiophene core substituents) with various imide substituents. RF7b shows a more intense absorption in the UV than RF7H and RF7a, due to the styryl groups. The low energy absorption maxima of both RF7H and RF7b

were red-shifted by about 10 nm compared to RF7a, indicating that hydrogen and styryl imide substituents have a similar effect on the optical properties of the core-NDI. The emission maximum (spectra in the Supporting Information Section, Figure S15) of RF7b was also red-shifted by 10 nm compared to RF7a. A similar trend was observed with the RF8 series (alkylamino core substituents, Figure 1B), but the red-shift was much smaller. The low energy absorption maxima and onsets of RF8H and RF8b red-shifted by only 2 nm compared to those of RF8a, whereas the emission maximum of RF8b red-shifted by 3 nm compared to that of RF8a. We believe that the smaller impact of the imide substituents on optical properties in solution for RF8 series is due to the stronger effect of the amino core substituents on the frontier molecular orbitals of NDI than the thiophene core substituents. The alkylamino core substituents therefore govern the optical properties of RF8 compounds in solution.

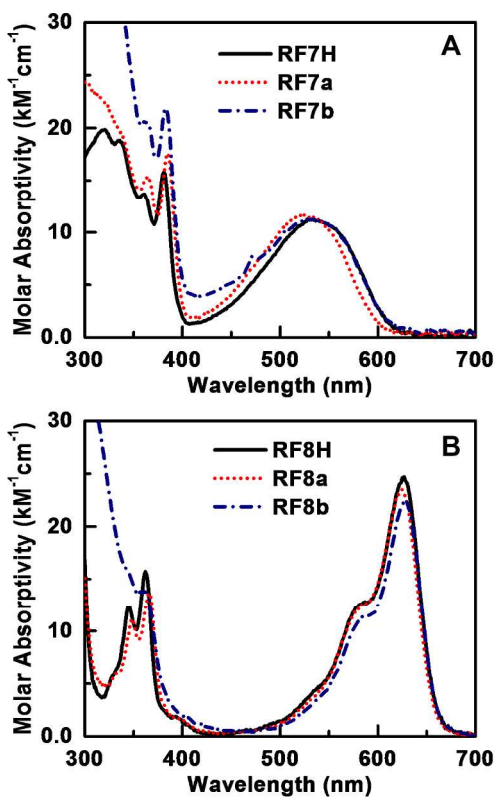


Fig. 1 Absorption spectra in chloroform solution of A) RF7 series ($[\text{RF7H}] = 2.8 \times 10^{-6} \text{ M}$, $[\text{RF7a}] = 1.9 \times 10^{-6} \text{ M}$, $[\text{RF7b}] = 1.9 \times 10^{-6} \text{ M}$); B) RF8 series ($[\text{RF8H}] = 2.1 \times 10^{-6} \text{ M}$, $[\text{RF8a}] = 2.0 \times 10^{-6} \text{ M}$, $[\text{RF8b}] = 2.0 \times 10^{-6} \text{ M}$).

Table 1 Optical properties in solution and film.

	Solution (chloroform)				Film		
	$\lambda_{\text{max}}^{\text{ems}}$ (nm)	$\lambda_{\text{max}}^{\text{abs}}(\epsilon)$ (nm, $\text{kM}^{-1}\text{cm}^{-1}$)	$\lambda_{\text{onset}}^{\text{abs}}$ (nm)	$^{\text{a}}E_{\text{gap,sol}}$ (eV)	$\lambda_{\text{max}}^{\text{abs}}(\epsilon)$ (nm, kcm^{-1})	$\lambda_{\text{onset}}^{\text{abs}}$ (nm)	$^{\text{a}}E_{\text{gap,film}}$ (eV)
RF7H	–	381 (15.8) 534 (11.2)	613	2.02	–	–	–
RF7a	625	384 (17.6) 524 (11.7)	600	2.07	392 573	625	1.98
RF7b	635	383 (21.9) 531 (11.3)	611	2.03	395 512	592	2.09
RF8H	–	362 (15.7) 586 (12.7) 627 (24.7)	659	1.88	–	–	–
RF8a	653	366 (13.7) 585 (12.6) 625 (23.5)	657	1.89	373 576 607	668	1.86
RF8b	656	361 (14.1) 586 (11.2) 627 (22.6)	659	1.88	365 563 652	762	1.63
RF6 ^b	653	364 (17.2) 583 (12.2) 627 (24.9)	659	1.88	365 576 611	677	1.83

a. Calculated using the $\lambda_{\text{onset}}^{\text{abs}}$ value. b. From ref. 8.

The solution and film UV/visible absorption spectra are compared for RF7a and RF7b in Figure 2A. The thin films were made by spin-coating. Homogeneous films with measurable absorbance could not be made with RF7H due to its limited solubility in organic solvents. The low energy absorption band of RF7a red-shifted by 49 nm going from solution to film (Table 1), and gained vibronic structure. The lower energy absorption maximum of RF7b blue shifted upon film formation by 19 nm, and gained some vibronic structure. In addition, the high energy band slightly red-shifted and became more intense relative to the low energy band. In the case of RF8a, the low energy band of RF8a blue-shifted upon film formation from 625 nm to 607 nm, and the shoulder peak near 580 nm became dominant. On the other hand, the low energy band of RF8b significantly broadens upon film formation, resulting in an unusually broad (500 nm – 800 nm) absorption for a NDI-based molecule. These experiments were repeated several times and the results were obtained reproducibly. The maximum low energy absorption for RF8b also red-shifts from 627 nm to 657 nm, and the high energy absorption band becomes more intense relative to the low energy absorption band, as seen for RF7b. The film optical gaps were 1.98 eV, 2.09 eV, 1.86 eV, and 1.63 eV for RF7a, RF7b, RF8a and RF8b, respectively. In films, both the core and imide substituents strongly influenced the absorption spectra, consistent with the substituents influencing molecular packing in the solid state.

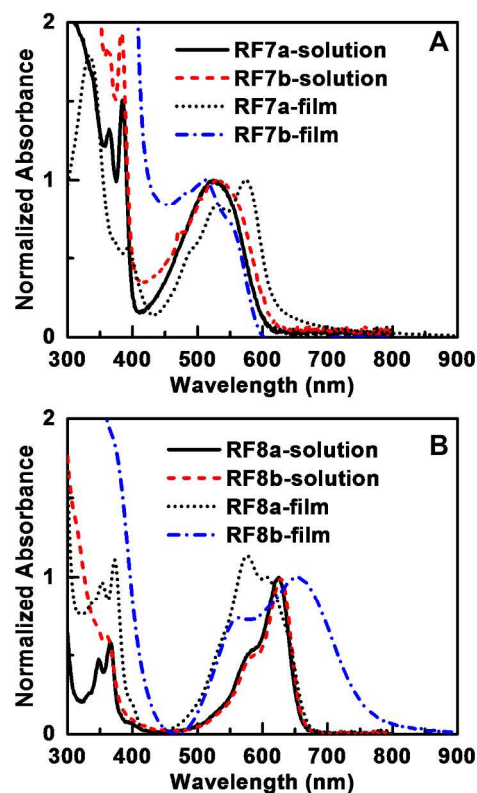


Fig. 2 Comparison of solution and thin film absorption spectra of A) RF7a and RF7b; B) RF8a and RF8b.

The spectra were normalized, setting the low energy absorption band to 1. (Absorption spectra of films were corrected for scattering and the details are available in supporting information)

Electrochemical properties.

Cyclic voltammograms and electrochemical properties for RF7 series and RF8a-b in solution are summarized in Figure 3 and Table 2. Cyclic voltammograms of RF8H could not be obtained due to limited solubility in dichloromethane. The RF7 molecules showed two reversible reductions and a single irreversible oxidation, whereas the RF8a-b molecules showed two reversible reductions and two reversible oxidations. These results are consistent with the literature for NDI compounds with similar core substituents.^{7,8,23} The RF8 molecules were harder to reduce and easier to oxidize than the corresponding RF7 molecules, due to the strong electron donating strength of the alkylamino core-substituents.

The $E_{1/2}$ values (vs. Fc/Fc^+) for the first reduction waves were -0.99 V, -1.09 V and -1.00 V for RF7H, RF7a and RF7b, respectively. Therefore, RF7b and RF7H are slightly easier to reduce than RF7a. RF7a is harder to reduce due to the inductive electron donating effect of the alkyl imide groups, which decreases the electron withdrawing strength of the carbonyls. Styryl and hydrogen imide substituents had a similar effect on the 1st reduction potential. The oxidation onset was also similar for styryl and hydrogen, and cathodically shifted for alkyl imide substituents. The first reduction potentials for RF8a and RF8b were -1.43 V and -1.37 V, respectively. As for the RF7 series, the molecule with styryl imide substituent was easier to reduce than with alkyl imide substituent. However, the difference between the first reduction potentials of alkyl versus styryl substituents was smaller for the RF8 series than for the RF7 series: The first reduction potential shifted anodically by 60 mV and 90 mV for the RF8 and RF7 series, respectively. The imide substituents affected the oxidations of RF8 molecules, with RF8b being slightly harder to oxidize than RF8a.

Table 2 Electrochemical properties

	$E_{1/2}^{ox}$ (V vs Fc/Fc^+)	$E_{1/2}^{red}$ (V vs Fc/Fc^+)
RF7H	Irreversible Onset: 1.14	-0.99, -1.38
RF7a	Irreversible Onset: 1.09	-1.09, -1.50
RF7b	Irreversible Onset: 1.13	-1.00, -1.36
RF8a	0.58, 1.06	-1.43, -1.82
RF8b	0.64, 1.10	-1.37, -1.72
RF6 ^c	0.62, irreversible	-1.36, -1.75

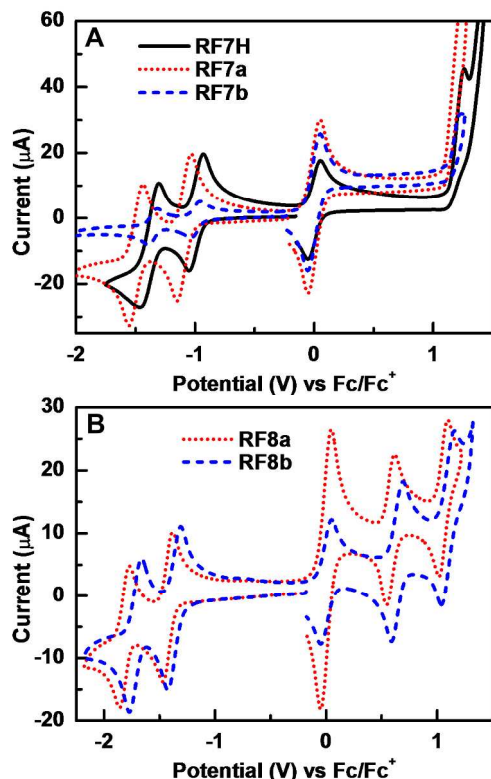


Fig. 3 Cyclic voltammograms in dichloromethane solution of A) RF7 series; B) RF8 series.

To better relate our results with the literature, we compare the cyclic voltammograms of RF8a and RF8b with that of our previously published RF6 in Figure 4. RF6 is a similar 2,6-dialkylamino-core substituted NDI but with 4-thienylphenyl imide substituents. The first reduction potential of RF6 is very similar to RF8b and is 70 mV more anodic (positive) than RF8a (with alkyl imide substituents). This indicates that both 4-thienylphenyl and styryl have a similar effect on the electronic properties of NDI. Gawrys et al reported a larger difference of 120 mV between the first reduction potentials of NDI (no core substituents) with alkyl and thienylphenyl imide substituents.³ Since the effect of imide substituents was smaller for our core-substituted NDI, we hypothesize that the effect of core substituents competes with that of imide substituents. The second reduction potentials of RF6 and RF8b were cathodically shifted from that of RF8a by 70 mV and 100 mV, respectively. This suggests that the styryl groups are slightly better at stabilizing the dianion than the 4-thienylphenyl groups.

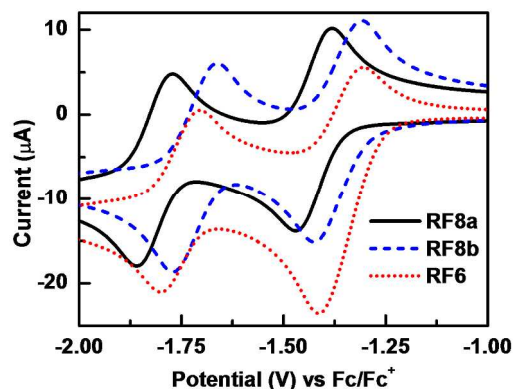


Fig. 4 Reduction waves of 2,6-dialkylamino core-substituted NDI with various imide substituents: 2-ethylhexyl (RF8a), styryl (RF8b) and 4-thienylphenyl (RF6).

DFT calculations.

To better understand the optical and electrochemical results, we performed hybrid density functional theory (DFT) calculations at the B3LYP/6-31G(d,p) level. Details of the calculations are available in the Supporting Information section. Figure 5 shows the optimized geometries for RF7b and RF8b. It is clear from the side views that RF7b is not as planar as RF8b. The dihedral angle between the NDI plane and the thiophene core substituents was 42° . To determine how much energy would be required to force the thiophene to be in-plane with the NDI core, we performed calculations where the dihedral angle between cNDI and the thiophene core substituent was varied (Figure S26 in Supporting Information section, both for gas and solution phase). We find that the dihedral angle between NDI and thiophene can easily vary between 30° and 100° , but the cost to have the thiophene planar with NDI is at least 15 kcal/mol, which is unlikely to occur.²⁴ Conversely, all substituents on RF8b are planar with the NDI plane (except the alkyl groups). We performed calculations where the dihedral angle between cNDI and styryl was varied for RF7b and RF8b (Figure S27, S28, both for gas and solution phase). For both RF7b and RF8b, the preferred orientation of the styryl group is in the same plane, or nearly in the same plane, as the cNDI plane. The cost to have the styryl group perpendicular to the cNDI plane is greater than 10 kcal/mol, making it unlikely to occur. We recognize that these geometries calculated for gas and

chloroform solution phase do not predict solid state geometries, however, they do give some idea of the geometry preferences for these types of molecules, and suggest that RF8b is more likely to adopt a fully planar geometry than RF7b.

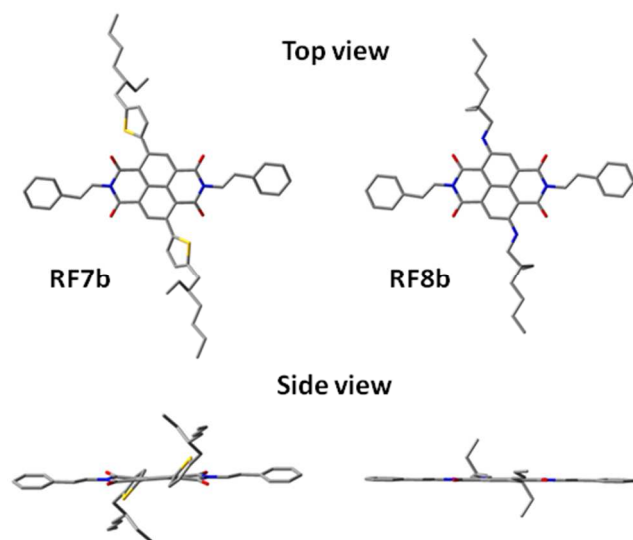


Fig. 5 Top and side view of optimized geometries of RF7b and RF8b at B3LYP/6-31G(d,p) level of theory (obtained in gas-phase. The optimized geometries obtained in chloroform solution were similar).

Figure 6 shows the electrostatic potential (ESP) surfaces of the two series of molecules. In these maps, positive potentials indicate electron-deficient regions (blue) and negative potentials indicate electron-rich regions (red). The images show that the NDI cores of RF8 molecules are more electron-rich than the corresponding RF7 molecules, consistent with the alkylamino groups being more electron-donating than the thiophene groups on the core. The alkyl imide substitution (RF7a, RF8a) increased the electron density of the NDI core compared to unsubstituted imides (RF7H and RF8H), demonstrating the positive inductive effect of alkyl imide units. On the other hand, the styryl imide groups (RF7b, RF8b) did not significantly change the electron density of the NDI core compared to unsubstituted imides (RF7H and RF8H). These results are fully consistent with the electrochemical results.

The electrostatic potential surface maps also clearly show that the styryl and thienylphenyl imide groups have large regions of negative potential energy (electron-rich). These electron-rich aromatics are expected to strongly influence molecular packing arrangements of the cNDI molecules in film. Electrostatics of polarized pi systems have been shown to predict and understand interactions between aromatics, and face-to-face stacking of an electron-rich aromatics with an electron-poor aromatics has been shown to be favorable.²⁵ We therefore suspect that the styryl and thienylphenyl imide substituents will preferably stack with the electron-deficient NDI cores.

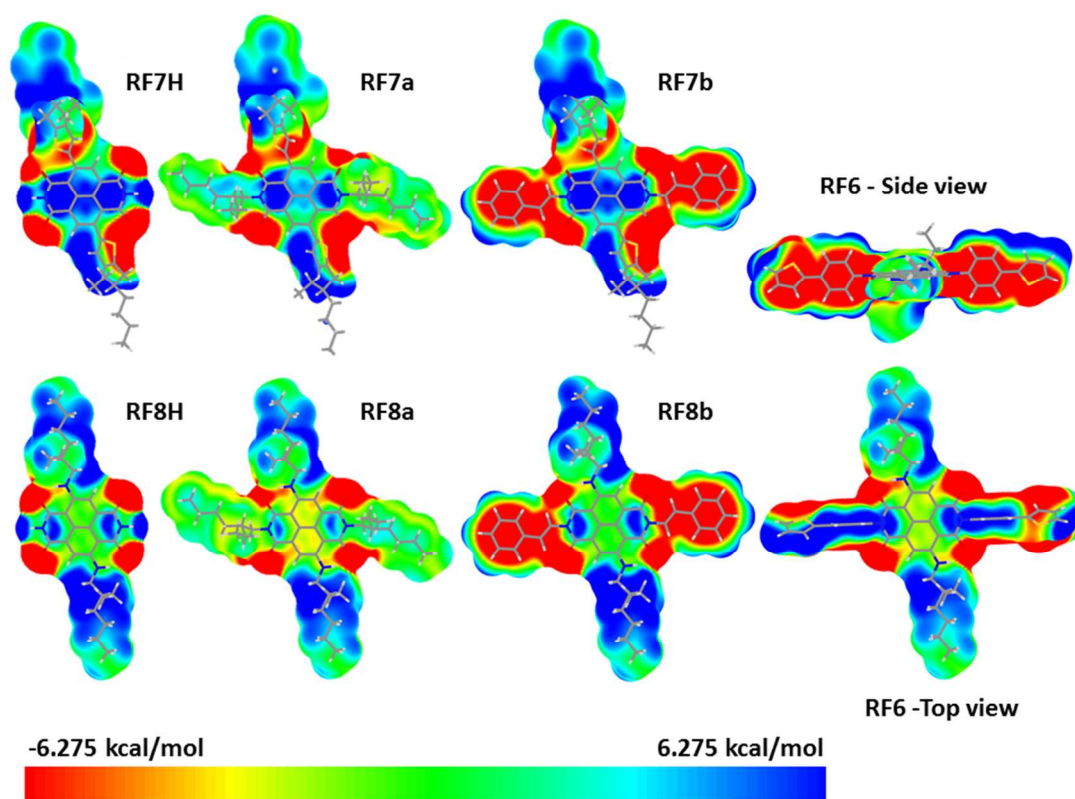


Fig. 6 Electrostatic potential surface maps of RF7 and RF8 series and RF6 calculated at the B3LYP/6-31G(d,p) level of theory.

To test this hypothesis, we optimized the geometry for a dimer of RF8b, shown in Figure 7. The dimer had a slipped face-to-face π -stacking with an angle of 23 degrees. This slipped J-type aggregation is consistent with the observed bathochromic shift upon film formation of RF8b. Furthermore, the electron-poor NDI core indeed stacked approximately face-centered with the electron-rich styryl imide substituents, resulting in donor-acceptor intermolecular interactions. The π -stacking distance between the NDI core and styryl unit was 3.3 Å, an ideal π -stacking distance for charge transport. Since both RF7b and RF6 have electron-rich imide substituents, we suspect that they will also have donor-acceptor type intermolecular interactions. Unfortunately, we were unable to calculate the optimized geometry for dimers of RF7b. Nevertheless, both RF7b and RF6 did not show unusually broad absorption in the visible range as RF8b did. We hypothesize that it may be because RF8b is planar whereas RF7b and RF6 are not completely planar. Further crystallography studies are required to better understand the relationship between structure, molecular packing and optical properties in the solid state.

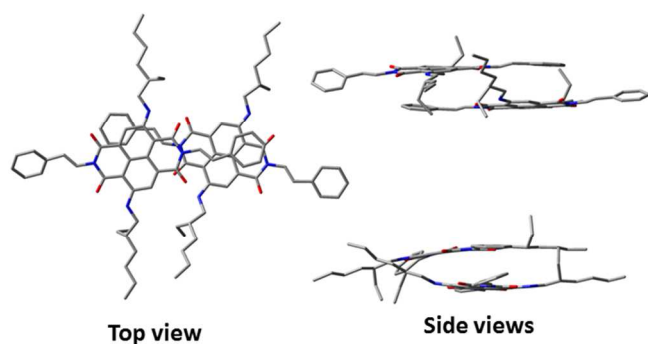


Fig. 7 Top and side views of optimized geometry of RF8b dimer in gas phase at M062x/6-31G(d,p) level of theory.^{26,27}

Conclusions

Studies of the series of cNDI molecules in solution and film led to several interesting findings. First, the effect of the imide substituents on the solution opto-electronic properties of NDI are reduced as

the electron donating strengths of the core substituent are increased, presumably because the stronger effect of core substituents overrides those of the imide substituents. Second, the combination of core and imide substituent strongly influenced the optical properties in the solid state by influencing molecular packing. Third, combining 2,6-alkylamino core substituents with styryl imide substituents lead to unusually broad absorption in the visible range for a cNDI molecule, probably due to a combination of planarity and aromatic donor-acceptor interactions between electron deficient NDI and electron rich styryl imide groups. Calculations suggest that RF8b assembles in a staggered fashion, with styryl imide groups stacked with NDI cores. This is also consistent with the unusually broad absorption spectra of FR8b in film for this type of molecule, with a low optical gap of 1.63 eV. This effect was not observed when using the thiophene core substituent (RF7b) or by using aryl imide substituents, presumably because the molecule cannot lay completely planar and will therefore adopt a different arrangement in the solid state. Crystal structures are required to further understand the results. Although imide substituents do not have a large impact on the opto-electronic properties of core-substituted NDI molecules in solution, they strongly affect the properties in film and thus provide an important variable to tune properties for use in opto-electronic devices.

Acknowledgments

We thank the American Chemical Society Petroleum Research Fund (SPN00045) for funding this project. We thank Prof. Anthony Pearson for useful discussions, Prof. John Protasiewicz for facilitating cyclic voltammetry and the Case High Performance Computing Cluster for the allocation of computing time. This material is based upon work supported by the National Science Foundation under Grant No. MRI-0821515 (for the purchase of the MALDI-TOF/TOF).

Notes and References

Electronic Supplementary Information (ESI) available: Reaction conditions tested for Chan-Lam coupling reaction of RF8H, ^1H NMR spectra, MALDI-TOF mass spectra, emission spectra, and computational data (FMOs of all molecules, and cartesian coordinates, frequencies and energies of the optimized geometries).

- 1 N. Sakai, J. Mareda, E. Vauthey, S. Matile *Chem. Commun.* 2010, **46**, 4225-4237.
- 2 X. Zhan, F. Antonio, S. Barlow, T. J. Marks, M. A. Ratner, M. R. Wasielewski, S. R. Marder *Adv. Mater.* 2010, **23**, 268-284.
- 3 P. Gawrys, D. Djurado, J. Rimarcik, A. Kornet, D. Boudinet, J.-M. Verilhac, V. Lukes, I. Wielgus, M. Zagorska, A. Pron *J. Phys. Chem. B* 2010, **114**, 1803-1809.
- 4 P. Gawrys, D. Boudinet, M. Zagorska, D. Djurado, J.-M. Verilhac, G. Horowitz, J. Pecaud, S. Pouget, A. Pron *Synth. Met.* 2009, **159**, 1478-1485.
- 5 S. K. Lee, Y. B. Zu, A. Herrmann, Y. Geerts, K. Mullen, A. J. Bard *J. Am. Chem. Soc.* 1999, **121**, 3513-3520.
- 6 R. S. K. Kishore, O. Kel, N. Banerji, D. Emery, G. Bollot, J. Mareda, A. Gomez-Casado, P. Jonkheijm, J. Huskens, P. Maroni, M. Borkovec, E. Vauthey, N. Sakai, S. Matile *J. Am. Chem. Soc.* 2009, **131**, 11106-11116.
- 7 E. Ahmed, G. Ren, F. S. Kim, E. C. Hollenbeck, S. A. Jenekhe *Chem. Mat.* 2011, **23**, 4563-4577.
- 8 R. Fernando, Z. Mao, E. Muller, F. Ruan, G. Sauvé *J. Phys. Chem. C* 2014, **118**, 3433-3442.
- 9 C. Xia, X. Fan, J. Locklin, R. C. Advincula *Org. Lett.* 2002, **4**, 2067-2070.
- 10 Y. Jiang, D. Yu, L. Lu, C. Zhan, D. Wu, W. You, Z. Xie, S. Xiao *J. Mater. Chem. A* 2013, **1**, 8270.
- 11 F. Chaignon, M. Falkenström, S. Karlsson, E. Blart, F. Odobel, L. Hammarström *Chem. Commun.* 2007, 64.
- 12 R. E. Dawson, A. Hennig, D. P. Weimann, D. Emery, V. Ravikumar, J. Montenegro, T. Takeuchi, S. Gabutti, M. Mayor, J. Mareda, C. A. Schalley, S. Matile *Nat. Chem.* 2010, **2**, 533-538.
- 13 C. Thalacker, C. Roeger, F. Wuerthner *J. Org. Chem.* 2006, **71**, 8098-8105.

- 14 M. J. Frisch, G. W. T, H. B. Schlegel, G. E. Scuseria, M. A. Robb, J. R. Cheeseman, G. Scalmani, V. Barone, B. Mennucci, G. A. Petersson, H. Nakatsuji, M. Caricato, X. Li, H. P. Hratchian, A. F. Izmaylov, J. Bloino, G. Zheng, J. L. Sonnenberg, M. Hada, M. Ehara, K. Toyota, R. Fukuda, J. Hasegawa, M. Ishida, T. Nakajima, Y. Honda, O. Kitao, H. Nakai, T. Vreven, J. A. Montgomery, Jr, J. E. Peralta, F. Ogliaro, M. Bearpark, J. J. Heyd, E. Brothers, K. N. Kudin, V. N. Staroverov, R. Kobayashi, J. Normand, K. Raghavachari, A. Rendell, J. C. Burant, S. S. Iyengar, J. Tomasi, M. Cossi, N. Rega, J. M. Millam, M. Klene, J. E. Knox, J. B. Cross, V. Bakken, C. Adamo, J. Jaramillo, R. Gomperts, R. E. Stratmann, O. Yazyev, A. J. Austin, R. Cammi, C. Pomelli, J. W. Ochterski, R. L. Martin, K. Morokuma, V. G. Zakrzewski, G. A. Voth, P. Salvador, J. J. Dannenberg, S. Dapprich, A. D. Daniels, Ö. Farkas, J. B. Foresman, J. V. Ortiz, J. Cioslowski, D. J. Fox In *Gaussian, Inc.* Wallingford CT, 9.
- 15 R. Dennington, T. Keith, J. Millam *GaussView*; Semichem Inc.: Shawnee Mission, KS, 2009.
- 16 A. D. Becke *J. Chem. Phys.* 1993, **98**, 5648-5652.
- 17 P. J. Stephens, F. J. Devlin, C. F. Chabalowski, M. J. Frisch *J. Phys. Chem.* 1994, **98**, 11623-11627.
- 18 P. Lam, C. G. Clark, S. Saubern, J. Adams, M. P. Winters, D. M. Chan, A. Combs *Tetrahedron Lett.* 1998, **39**, 2941-2944.
- 19 W. W. K. R. Mederski, M. Lefort, M. Germann, D. Kux *Tetrahedron* 1999, **55**, 12757-12770.
- 20 K. S. R. T.-S. Wu, T.-S. Wu *Tetrahedron* 2012, **68**, 7735-7754.
- 21 E. T. Chernick, M. J. Ahrens, K. A. Scheidt, M. R. Wasielewski *J. Org. Chem.* 2005, **70**, 1486-1489.
- 22 D. M. T. Chan, K. L. Monaco, R.-P. Wang, M. P. Winters *Tetrahedron Lett.* 1998, **39**, 2933-2936.
- 23 R. Fernando, Z. Mao, G. Sauve *Org. Electron.* 2013, **14**, 1683-1692.
- 24 E. V. Anslyn, D. A. Dougherty In *Modern physical organic chemistry*; University Science Books: Sausalito, California, 2006, p 92-128.
- 25 C. R. Martinez, B. L. Iverson *Chem. Sci.* 2012, **3**, 2191-2201.

- 26 Y. Zhao, D. G. Truhlar *Theor. Chem. Account* 2007, **120**, 215-241.
- 27 Y. Zhao, D. G. Truhlar *J. Chem. Phys.* 2006, **125**, 194101.